Formation and Maintenance Mechanisms of the Stable Layer over the Po Valley during MAP IOP-8

ALLISON M. HOGGARTH, HEATHER DAWN REEVES, AND YUH-LANG LIN

Department of Marine, Earth, and Atmospheric Sciences, North Carolina State University, Raleigh, North Carolina

(Manuscript received 11 October 2005, in final form 24 February 2006)

ABSTRACT

During intensive observation period 8 (IOP-8) of the Mesoscale Alpine Program, a strong stable layer formed over Italy's Po Valley and the northern Ligurian Sea. This stable layer has been shown in previous research to be important for the formation of convection over the Ligurian Sea and the lack thereof over the Po Valley and southern slopes of the Alps. The purpose of this study is to investigate the mechanisms that acted to form and maintain the stable layer during IOP-8. This aim is accomplished through inspection of observed data as well as numerical simulations and sensitivity experiments. Observations and reanalysis data show that starting on 17 October 1999, a relatively cool, stable air mass was advected around the eastern side of the Alps into the lower atmosphere of the Po Valley. Both observational data and model output show this air mass as being blocked as it encountered the western Alps, thus resulting in an accumulation of cool, stable air at low levels in the Po Valley during the ensuing 60 h. When southerly flow approached northern Italy beginning on 20 October 1999, both the western Alps and the northern Alps appeared to help retain the low-level, cool, stable air over the Po Valley. A trajectory and sounding analysis shows that warmer, less stable air originating from over the southern Mediterranean Sea was advected atop the low-lying stable layer within the Po Valley. It is hypothesized that this differential advection, as well as blocking by the western and northern flanks of the Alps, were responsible for the longevity of the stable layer. A series of numerical simulations and sensitivity experiments were performed to test the above hypotheses. These tests support the hypotheses. Other mechanisms were also considered, including blocking of solar radiation by clouds, friction, and evaporative cooling. These simulations revealed that all three processes were critical for the longevity of the stable layer and point to the importance of accurate model representation of subgrid-scale processes.

1. Introduction

To develop a better understanding of flow modification by the Alps, the Mesoscale Alpine Program (MAP) was launched in the fall of 1999 with one of the main goals being to improve our understanding of the dynamical and physical processes that control precipitation over complex topography. One of the MAP intensive observation periods (IOPs) that has received much attention is IOP-8 (20–21 October 1999). Both the Swiss Model and the Mesoscale Compressible Community (MC2) model forecast moderate-to-heavy precipitation accumulations to occur (greater than 100 mm) over the Lago Maggiore Target Area (LMTA; Fig. 1) on 21 October 1999 (Bousquet and Smull 2003). Indeed, IOP-8 was characterized by many ingredients common to heavy orographic precipitation events (Lin et al. 2005), including an impeded, preexisting convective system and strong low-level jet that advected relatively moist, convectively unstable air toward the mountain range. However, the observed precipitation amounts for IOP-8 were much less than anticipated, with maximum values averaging between 30 and 50 mm across the LMTA. Well south of the target area, over the Po Valley and Ligurian Sea, precipitation was heavier with rain rates exceeding 80 mm in 24 h (Bousquet and Smull 2003). This convective development was not anticipated by the forecast models (Bousquet and Smull 2003).

IOP-8 departed from typical cases of heavy orographic precipitation in that there was significant cold air damming over the Po Valley that extended southward over the northern Ligurian Sea (Medina and Houze 2003; Rotunno and Ferretti 2003; Bousquet and

Corresponding author address: Yuh-Lang Lin, Dept. of MEAS, NCSU, 1125 Jordan Hall, Faucette Dr., Raleigh, NC 27695-8208. E-mail: yl_lin@unity.ncsu.edu

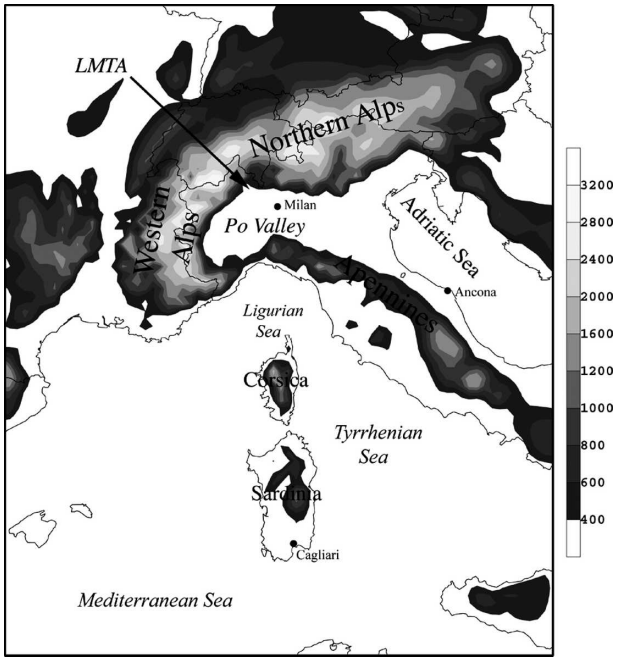

FIG. 1. Alps topography (m; shaded as in legend) showing the sounding locations of Milan, Cagliari, and Ancona. The LMTA is also indicated.

Smull 2003; Lin et al. 2005). This stable layer, which initially started to form on 17 October 1999 and persisted throughout the duration of IOP-8, has been shown to have a profound effect on the flow fields and precipitation distribution during IOP-8. For example, Lin et al. (2005) noted that lifting along the leading edge of the stable layer was sufficient to trigger convection over the Ligurian Sea. Reeves and Lin (2006) showed that the strength and horizontal extent of the stable layer was incorrectly forecast by the MC2 model (see their Fig. 4). Smull et al. (2001) suggested that the incorrect forecast in precipitation for IOP-8 was due to this underestimation of the depth and extension of the blocked flow. Reeves and Lin (2006) showed through their idealized simulations that as the strength of the inversion over the Po Valley and upstream of the Apennines is increased, the location of maximum convection is shifted southward.

Despite its apparent influence on the flow fields and precipitation distribution, the factors contributing to the formation, maintenance, and demise of the stable layer during IOP-8 have received relatively little attention from the scientific community. Understanding of the mechanisms important for the longevity of the stable layer and how these mechanisms affect precipitation distribution has relevance not only for the southern Mediterranean region, but for other regions as well. For example, Grossman and Durran (1984) noted that blocking upstream of the Western Ghats in India can affect the formation of offshore convective systems. Houze and Medina (2005) and Medina et al. (2005) noted the importance of orographic blocking in the formation of shear-induced convection upstream of the Cascade Mountains in Oregon as well as upstream of the Alps. Neiman et al. (2002) demonstrated that blocking upstream of the coastal mountains in California can also have a profound impact on the formation of convection. Finally, Kusunoki et al. (2004) showed that blocking along the central mountain range of Japan can alter the precipitation field.

The main focus of this research is to determine what forcings caused the stable layer during IOP-8 to develop, to persist for such an extended period of time, and to finally erode. Herein, we also investigate how the precipitation distribution during IOP-8 was affected by these different forcings. This paper is organized as follows. In section 2, the evolution of pertinent synoptic and mesoscale flow features is presented. Section 3 provides the model description and experiment design. Section 4 examines the formation and maintenance mechanisms of the stable layer over the Po Valley through numerical sensitivity experiments. The conclusions are discussed in section 5.

2. Synopsis of the IOP-8 environment

Figure 2 shows the evolution of sea level pressure, 925-hPa equivalent potential temperature θ_e, and winds from 1200 UTC 17 October to 1200 UTC 21 October 1999. These analyses are taken from the 40-yr European Centre for Medium-Range Weather Forecasts (ECMWF) Re-Analysis (ERA-40) 0.5° data. Note that there are wind barbs and θ_e values contoured over the orography where the 925-hPa surface intersects the orography. This is an artifact of the software program used to make the figure [General Environmental Meteorological Package (GEMPAK; Koch et al. 1983)], which assumes a standard atmospheric lapse rate and constant winds for pressure surfaces that intersect terrain. This is the case for all subsequent figures presented in this paper as well.

At 1200 UTC 17 October (Fig. 2a), a high pressure center was positioned over northeastern Europe that advected low-θ_e air into the Po Valley. By 1200 UTC 18 October (Fig. 2b), the low-θ_e air had spread across the Po Valley, all the way to the western Alps. Low-θ_e air continued to accumulate along the western Alps during the following 48 h (Fig. 2c). Although it is not apparent in Figs. 2b and 2c given the resolution of the reanalysis data, the more detailed analyses presented in Medina and Houze (2003; see their Figs. 4b and 5b) show that

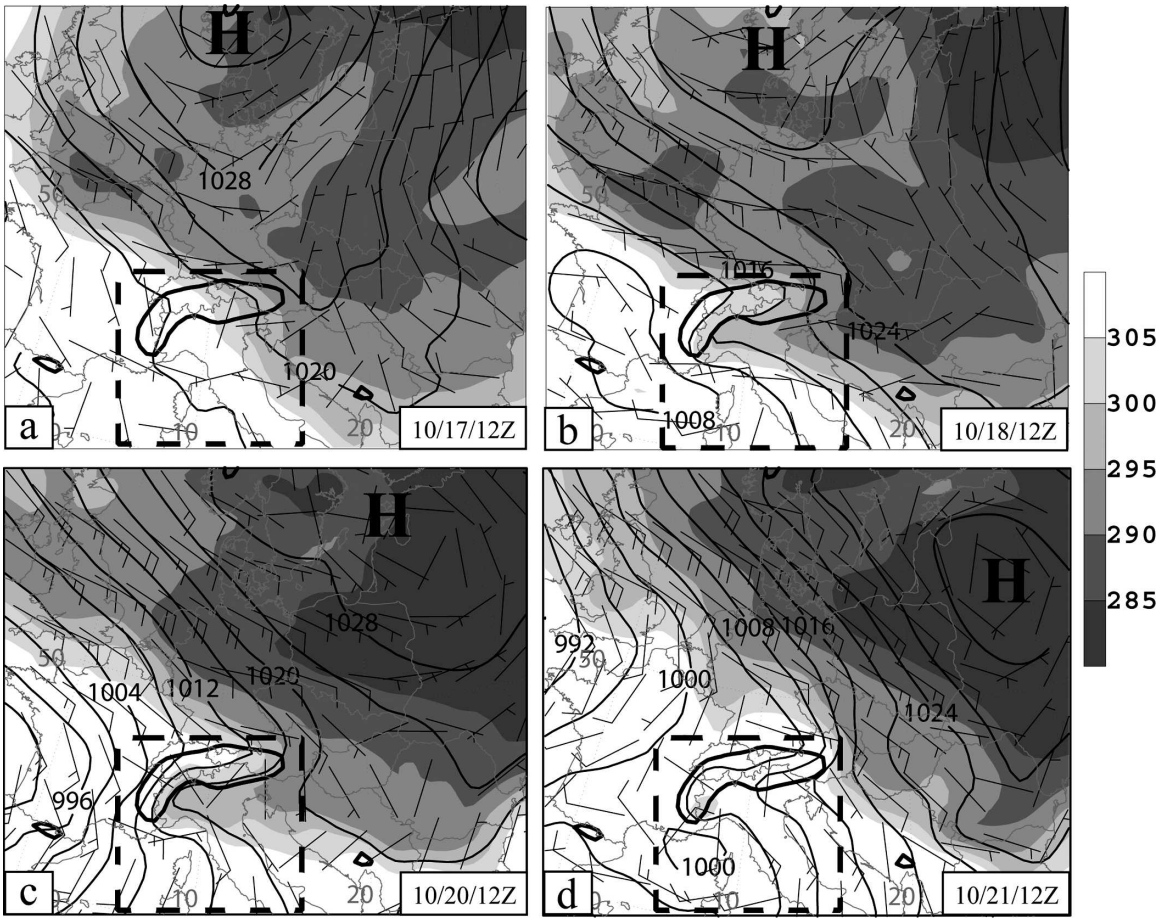

FIG. 2. The ERA-40 0.5° reanalysis data showing mean sea level pressure (hPa; contoured), 925-hPa θ_e (K; shaded as in legend) and 925-hPa wind barbs (one-half barb is 5 m s^{-1}) at (a) 1200 UTC 17 Oct, (b) 1200 UTC 18 Oct, (c) 1200 UTC 20 Oct, and (d) 1200 UTC 21 Oct. The 1-km terrain height is given by the thick contours. The thick dashed square denotes the region plotted in Fig. 7.

along the western Alps, the winds were northerly, indicative of blocking by this portion of the range. Medina and Houze (2003), Rotunno and Ferretti (2003), Bousquet and Smull (2003), and Lin et al. (2005) have all suggested that orographic blocking by the western Alps acted to form and help maintain the stable layer. By 1200 UTC 20 October (Fig. 2c), the high pressure center over northeastern Europe had shifted eastward so that higher-θ_e air originating from over the Adriatic Sea was advected toward the northern Alps. As this southerly airstream encountered the northern Alps, it appeared to be blocked and deflected westward into the Po Valley (see Fig. 5b of Medina and Houze 2003). This apparent deflection of the higher-θ_e, southerly flow continued throughout the following 24 h so that by 1200 UTC 21 October (Fig. 2d), there was only a small pocket of low-θ_e air remaining along the western Alps. Another feature of note in Fig. 2 is the U-shaped bend of the isobars in the Po Valley. This ridging is similar to that observed in cases of cold air damming along the Appalachian Mountains (Bell and Bosart 1988).

Soundings taken at Milan, Italy, from 0000 UTC 18 October through 0600 UTC 22 October (see Fig. 1 for location) are shown in Fig. 3. At 0000 UTC 18 October (Fig. 3a), the wind barbs show that from the surface to about 800 hPa, the flow was easterly. This lowest 200-hPa layer was capped by a near-neutral layer that extended up to about 680 hPa. At 0000 UTC 20 October (Fig. 3b), the low-level flow was, again, from the east. There was a weak inversion capping this lowest layer of air, extending from about 880 to 720 hPa. Note that the temperatures in the lowest 100 hPa decreased an average of 4.5 K during this 48-h period. By 0000 UTC 21 October (Fig. 3c), the capping inversion had strengthened. This increase appears to be primarily due to the advection of warm air from the south over the stable layer. Note that between 0000 UTC 20 October and 0000 UTC 21 October, the temperatures between 800

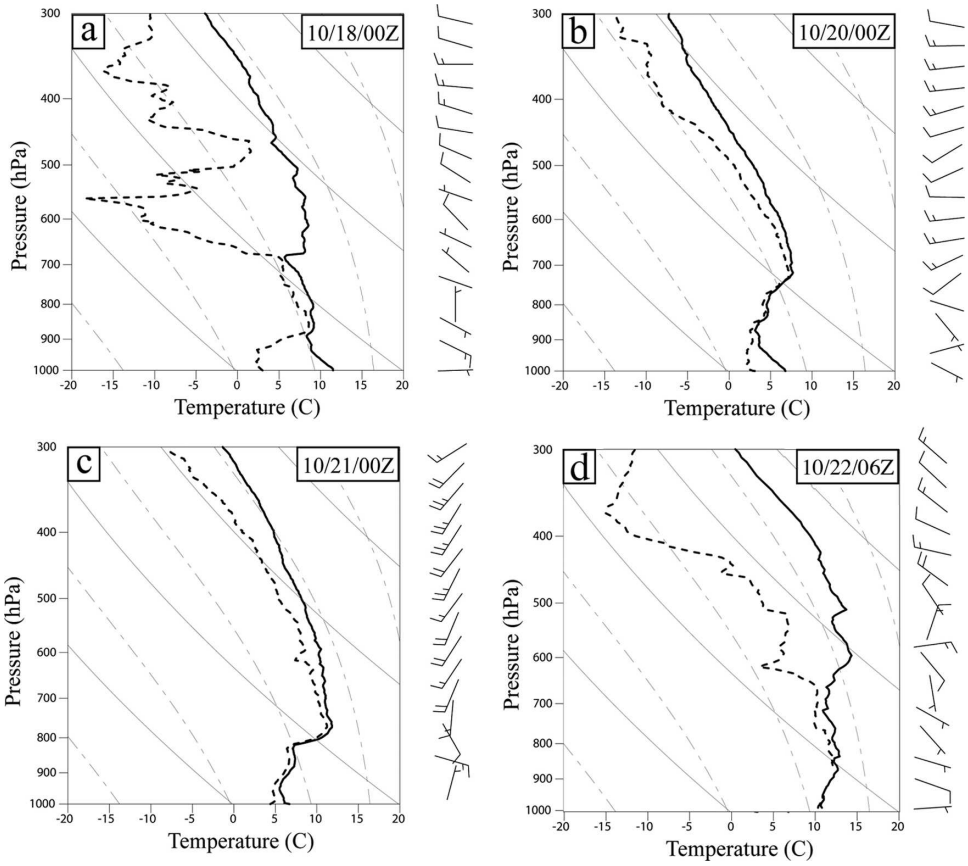

FIG. 3. Observed soundings from Milan at (a) 0000 UTC 18 Oct, (b) 0000 UTC 20 Oct, (c) 0000 UTC 21 Oct, and (d) 0600 UTC 22 Oct. Temperature is given by the solid lines and dewpoint temperature by the dashed lines. Wind speed and direction are denoted by the wind barbs to the right of each panel. One full barb is 10 m s^{-1}.

and 700 hPa increased about 5 K. This same phenomena was noted by Lin et al. (2005), who postulated that the differential advection of the warm air mass to the south over the cooler air mass in the Po Valley was responsible for the longevity of the stable layer, a mechanism consistent with that presented in Wolyn and McKee (1989). The fact that there was warm air advection above about 800 hPa allowed for the stable layer to persist until 0000 UTC 22 October (not shown). By 0600 UTC 22 October (Fig. 3d), it was mostly eroded.

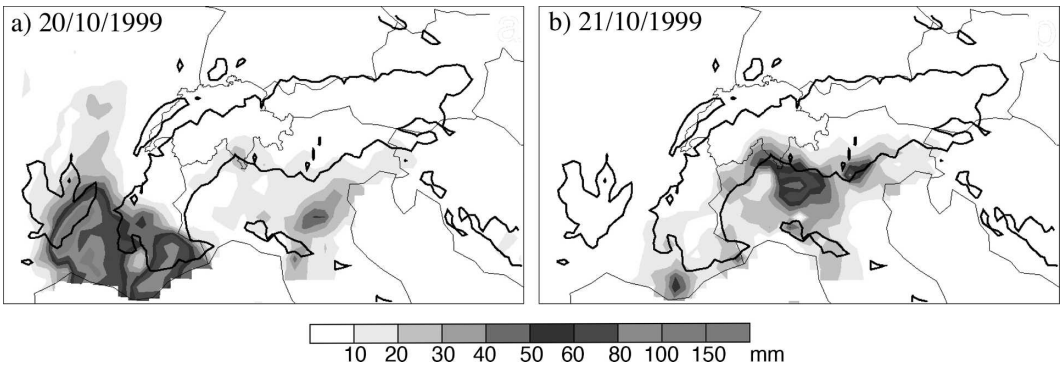

FIG. 4. The observed 24-h accumulated precipitation (mm; shaded as in legend) beginning at (a) 0600 UTC 20 Oct and (b) 0600 UTC 21 Oct.

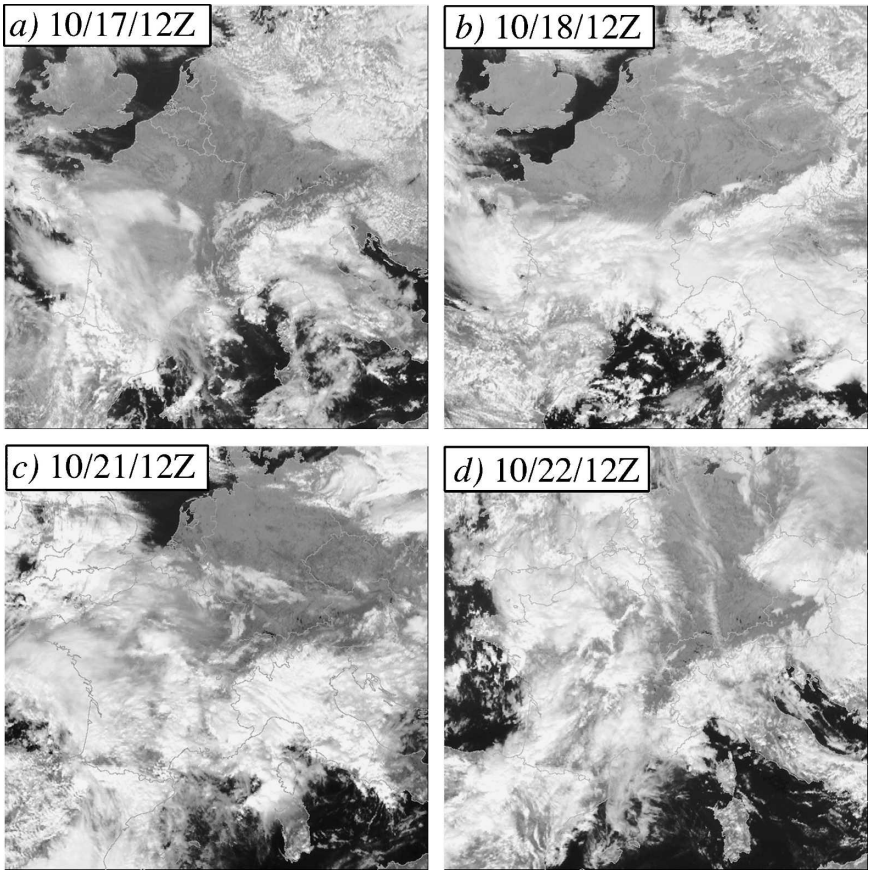

FIG. 5. Visible satellite imagery at (a) 1200 UTC 17 Oct, (b) 1200 UTC 18 Oct, (c) 1200 UTC 21 Oct, and (d) 1200 UTC 22 Oct.

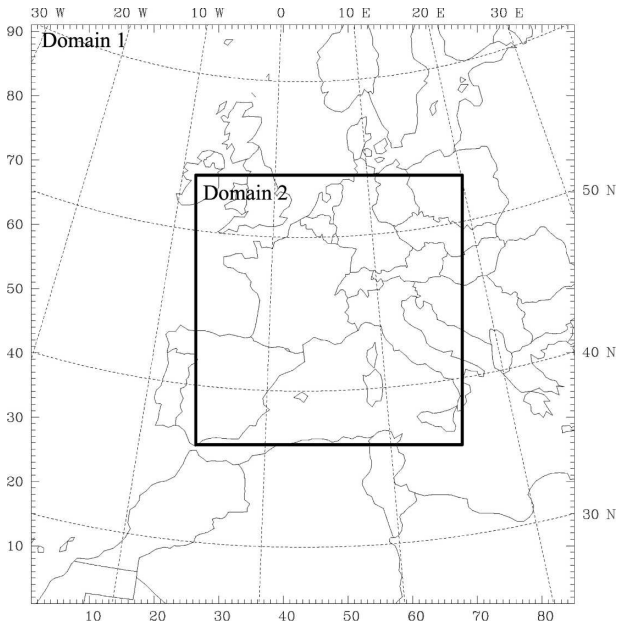

FIG. 6. Domains used in the MM5 simulations.

This erosion appears to be due to heating of the lowest 150 hPa, or so. In Fig. 3d, the temperatures in the lowest 100 hPa were an average of 5 K warmer than in Fig. 3c.

Bell and Bosart (1988) and Fritsch et al. (1992) argued that in cases of Appalachian cold air damming, diabatic effects including latent cooling and the blocking of solar radiation by clouds can be important maintenance mechanisms for cold air damming episodes. This notion was introduced as a possible mechanism for the maintenance of the stable layer during IOP-8 by Bousquet and Smull (2003) and Steiner et al. (2003). Inspection of the Milan soundings (Figs. 3b and 3c) shows that there was a slight cooling (about 1 K) and moistening (about 0.8 g kg^{-1}) beneath the inversion between 0000 UTC 20 October and 0000 UTC 21 October. Additionally, an examination of the 24-h accumulated precipitation for 20 and 21 October (Fig. 4) shows there was precipitation across the Po Valley during this period.

Inspection of the visible satellite imagery (Fig. 5)

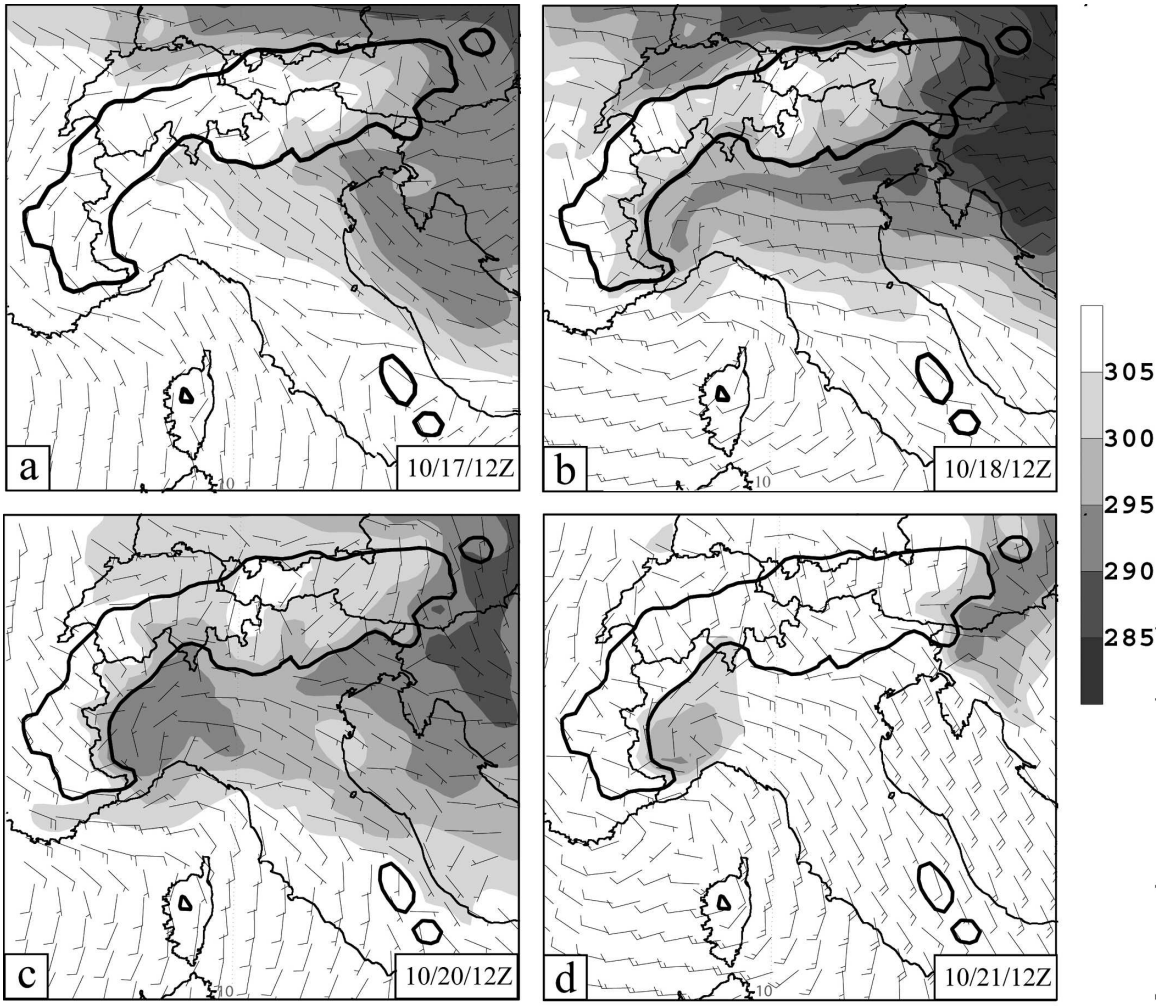

FIG. 7. MM5 CTRL-simulated 925-hPa θ_e (K; shaded as in legend) and wind barbs (one-half barb is 5 m s^{-1}) at (a) 1200 UTC 17 Oct, (b) 1200 UTC 18 Oct, (c) 1200 UTC 20 Oct, and (d) 1200 UTC 21 Oct. The 1-km terrain height is given by the thick contours.

shows that clouds began to form over the Po Valley at 1200 UTC 17 October (Fig. 5a) just as the stable layer was beginning to form. This cloud cover persisted over the Po Valley for the next 96 h as is demonstrated in Figs. 5b and 5c, which show the satellite imagery for 1200 UTC 18 October and 1200 UTC 21 October, respectively. By 1200 UTC 22 October (Fig. 5d), the cloud cover over the Po Valley had mostly dissipated. The fact that stable-layer formation and demise occurred concurrent with the formation and dissipation of clouds indicates that differential solar heating may have been responsible for the stable layer, or at least acted to enhance it.

To more definitively pinpoint the physical processes responsible for the formation, maintenance, and erosion of the stable layer, numerical sensitivity tests were employed.

3. Numerical simulation of IOP-8

a. Model description and experiment design

The numerical simulations were performed using version 3.6 of the fifth-generation Pennsylvania State University–National Center for Atmospheric Research (PSU–NCAR) Mesoscale Model (MM5; Dudhia 1993; Grell et al. 1994). This mesoscale model is nonhydrostatic and based on terrain-following sigma vertical coordinates. Two nested domains, with two-way interaction, were used for the simulations (Fig. 6). Domain 1 used 45-km grid spacing with 91 × 85 grid points in the horizontal and a terrain resolution of 19 km. Domain 2 used a 15-km grid spacing with 121 × 121 grid points and a 4-km terrain resolution. Forty-five unevenly spaced full-sigma levels were used in the vertical with the maximum resolution in the boundary layer. The

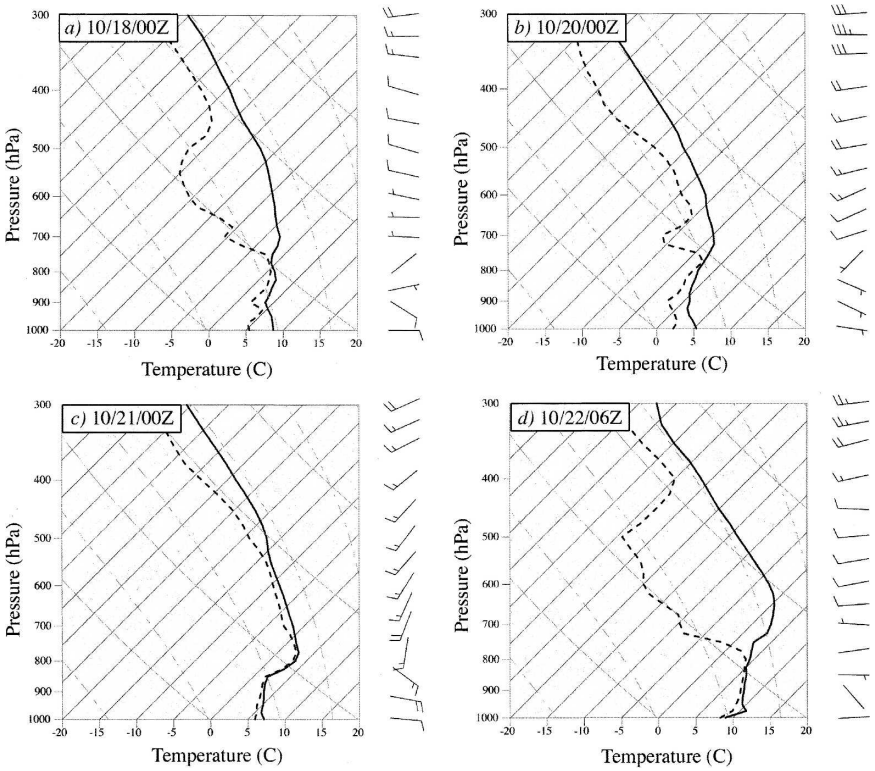

FIG. 8. CTRL soundings from Milan at (a) 0000 UTC 18 Oct, (b) 0000 UTC 20 Oct, (c) 0000 UTC 21 Oct, and (d) 0000 UTC 22 Oct. Temperature is given by the solid lines and dewpoint temperature by the dashed lines. Wind speed and direction are denoted by the wind barbs to the right of each panel. One full barb is 10 m s^{-1}.

time steps for domains 1 and 2 were 90 and 30 s, respectively. Data from ERA-40, which have a resolution of 2.5° × 2.5° latitude–longitude, were used to initialize the model and update the boundary conditions every 6 h. The model was initialized at 0000 UTC 17 October, with domain 2 initialized 6 h after domain 1, and integrated until 1200 UTC 22 October. The Betts–Miller (Betts and Miller 1993) cumulus parameterization scheme was used for domain 1, while domain 2 used the Grell (1993) cumulus parameterization scheme. For the microphysical parameterization scheme, the Goddard Lin–Farley–Orville scheme (Lin et al. 1983; Tao and Simpson 1993) was chosen and the Blackadar (1979) scheme was selected for the boundary layer parameterization. Output from domain 2 will be used in all subsequent figures and discussions unless otherwise noted.

b. Analysis of the control simulation

We first present a control simulation (CTRL) with all physical processes activated and actual orography present. This simulation was designed to capture the important flow features of IOP-8.

Figure 7 shows the CTRL-simulated 925-hPa θ_e and wind fields from 1200 UTC 17 October to 1200 UTC 21 October. As in the ECMWF reanalysis data (Fig. 2a), low-θ_e air associated with a high pressure region over northeastern Europe was advected into the Po Valley beginning at 1200 UTC 17 October (Fig. 7a). By 1200 UTC 18 October (Fig. 7b), this low-θ_e air mass had encountered the western Alps. The wind barbs in Fig. 6b show this air mass as being deflected to the south, around the western Alps. At 1200 UTC 20 October (Fig. 7c), the high pressure region over northeastern Europe had shifted toward the east (not shown) so that the flow entering the Po Valley originated over the Adriatic Sea. By 1200 UTC 21 October (Fig. 7d), the cold dome was mostly eroded and only a small pocket of low-θ_e air remained along the western Alps. Although it is not shown in Fig. 7, the movement and maximum pressure in the high pressure area of northeastern Europe were well reproduced in the CTRL simulation. However, the θ_e values within this high pressure region were moderately lower (between 2 and 3 K) than in the reanalysis data (not shown).

The model was generally able to reproduce the stable

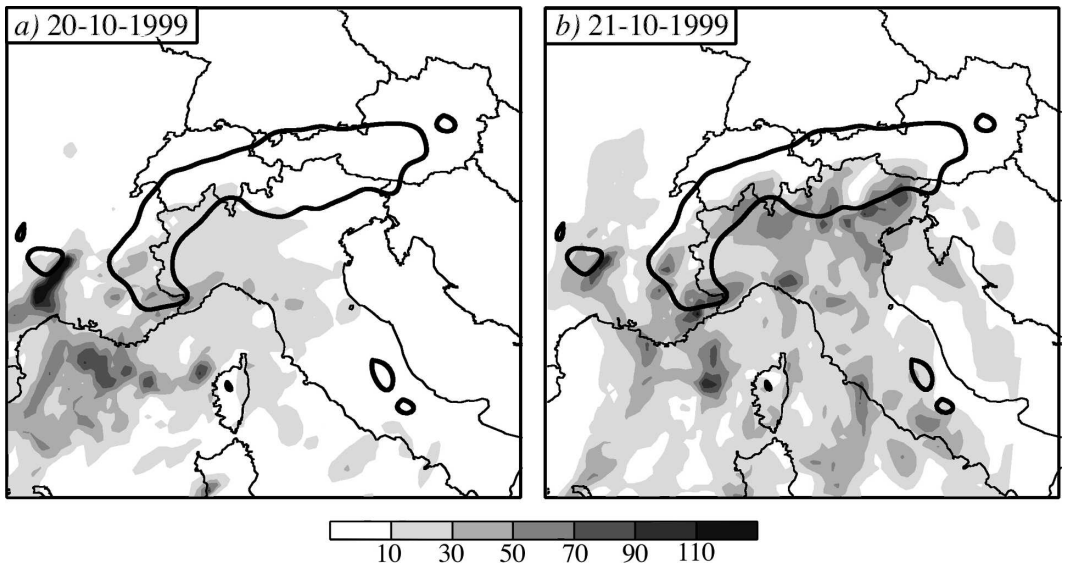

FIG. 9. CTRL-simulated 24-h accumulated precipitation (mm; shaded as in legend) on (a) 20 and (b) 21 Oct 1999.

layer depth, as seen in the simulated soundings from Milan in Fig. 8. At 0000 UTC 18 October (Fig. 8a), there was easterly flow in about the lowest 200 hPa. There was a near-neutral layer of air, similar to the observations (Fig. 3a) between about 900 and 750 hPa. Consistent with that shown in Fig. 7, the advection of cooler air across the Po Valley resulted in low-level temperatures at Milan that were about 2 K lower (Fig. 8b) than those observed (Fig. 3b) at 0000 UTC 20 October. Between 0000 UTC 20 October and 0000 UTC 21 October, the CTRL simulation experienced saturation of the lowest levels (Fig. 8c). The inversion height at 0000 UTC 21 October (Fig. 8c) compares well to the observed inversion height (Fig. 3c) as does the wind speed and direction both above and below the inversion. Also in Fig. 8c, a warmer, less stable air mass was positioned atop the cooler, more stable air in the surface layer, evidence of differential advection. Figure 8d shows that the stable layer had mostly eroded by 0600 UTC 22 October, consistent with the observations (Fig. 3d).

The CTRL-simulated 24-h accumulated precipitation for 20 and 21 October is shown in Fig. 9. Comparison of this figure to the observed precipitation accumulations (Fig. 4) shows generally good agreement on the locations of maximum precipitation. As was noted in Lin et al. (2005), there was a precipitation maximum of between 90 and 110 mm located northwest of Corsica, France, on 21 October (Fig. 9b). This maximum was positioned along the leading edge of the stable layer and appears to be associated with mechanical lifting of the incident, warm airstream by the cold dome. Figure 10 shows the CTRL-simulated cloud cover from 1200 UTC 17 October to 1200 UTC 21 October. Ac-

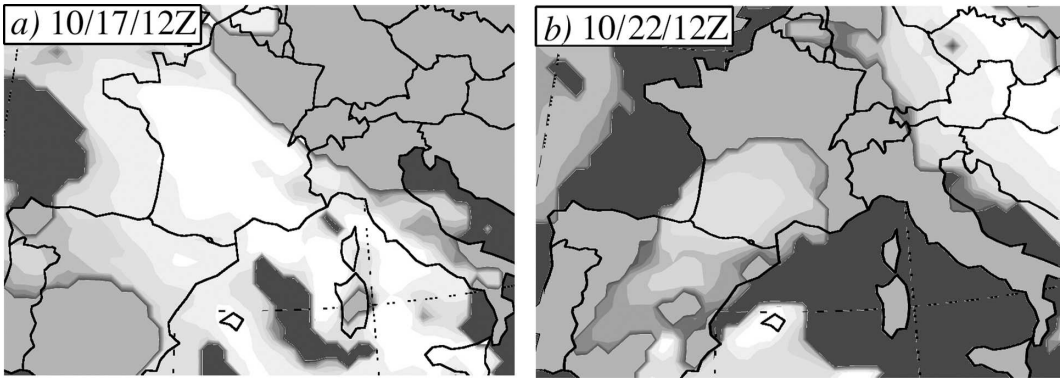

FIG. 10. CTRL-simulated cloud cover (derived from model output cloud-top temperatures) at (a) 1200 UTC 17 Oct and (b) 1200 UTC 22 Oct.

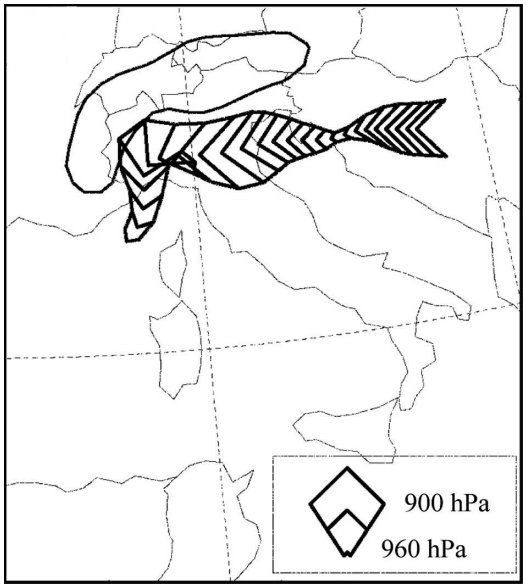

FIG. 11. CTRL-simulated backward air parcel trajectory starting at 1200 UTC 17 Oct and ending 0000 UTC 19 Oct at 950 hPa.

cording to this figure, the Po Valley was mostly free of cloud cover on 1200 UTC 17 October (Fig. 10a), but there was a large baroclinic leaf just west of the Po Valley that moved over the Po Valley during the following 24 h (Fig. 10b) and remained over the Po Valley until 0600 UTC 22 October (not shown). As in the observations, by 1200 UTC 22 October (Fig. 10b), the baroclinic leaf had moved eastward, past the Po Valley and the skies over the Po Valley were mostly clear.

Based on the comparison of the CTRL-simulated output (Figs. 7, 8, 9, and 10) with the ECMWF reanalysis fields and observations (Figs. 2, 3, 4, and 5), it appears the CTRL simulation reasonably reproduced the stable layer development across the Po Valley as well as other relevant flow features and will, therefore, be used for further investigation.

4. Formation and maintenance mechanisms

a. Blocking by the western Alps

The wind vectors in Fig. 7 indicate the western Alps blocked the impinging easterly flow between 1200 UTC 17 October and 0000 UTC 20 October. Figure 11 shows a backward trajectory of an air parcel ending at 0000 UTC 19 October at 950 hPa over the Ligurian Sea. This figure indicates that air parcels incident to the western Alps were blocked by the western Alps and deflected to the south. To more rigorously test the effects of blocking by the western Alps on stable layer development, a simulation was performed in which the western Alps were removed, while keeping everything else identical to the CTRL simulation. The modified terrain for this simulation can be viewed in Fig. 12. This simulation is referred to as the NOWA simulation.

Figure 12 shows the NOWA-simulated 925-hPa θ_e and wind fields. Until 0000 UTC 18 October, the agreement between the CTRL and NOWA simulations was very good (not shown). However, as there was no barrier in its path to deflect it toward the Ligurian Sea, the low-θ_e air continued to flow through northern Italy and into eastern France with the lowest-θ_e air remaining along the northern Alps (Fig. 12a). Southerly flow developed over Italy at 1200 UTC 20 October in the NOWA simulation (not shown) as in the CTRL simulation. This southerly flow was deflected toward the west as it impinged on the northern Alps, flushing the

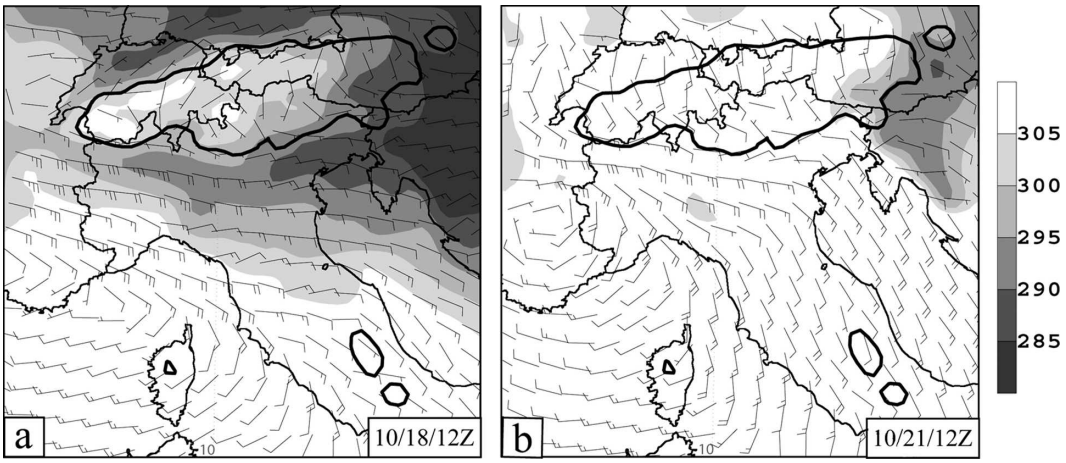

FIG. 12. NOWA-simulated 925-hPa θ_e (K; shaded as in legend) and wind barbs (one-half barb is 5 m s^{-1}) at (a) 1200 UTC 18 Oct and (b) 1200 UTC 21 Oct. The 1-km terrain height is given by the thick contours.

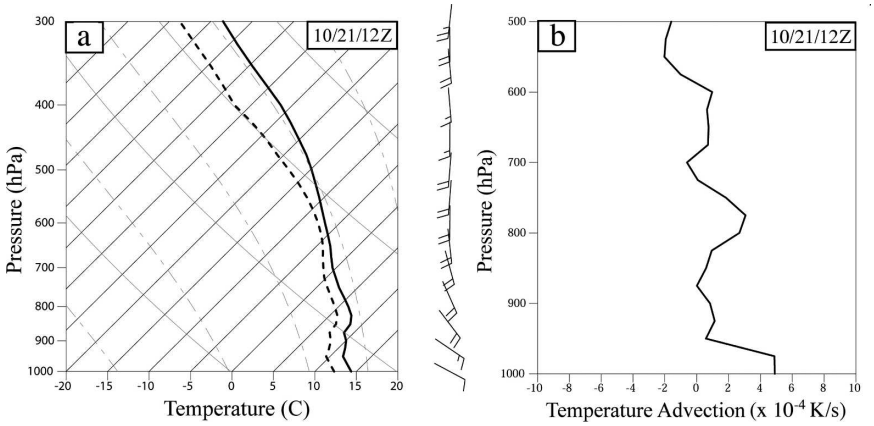

FIG. 13. NOWA-simulated (a) sounding (one full barb is 10 m s^{-1}) and (b) vertical profile of temperature advection ($\times 10^{-4}$ K s^{-1}) at Milan at 0000 UTC 21 Oct.

low-θ_e air mass out of the Po Valley by 1200 UTC 21 October (Fig. 12b).

Figure 13a, which shows the NOWA-simulated Milan sounding at 1200 UTC 21 October, reveals that the thermodynamic profile in the Po Valley was nearly moist neutral throughout most of the troposphere and the low-level flow was from the southeast. In fact, this sounding is similar to Milan soundings from IOP-2b (Rotunno and Ferretti 2003) and the 1996 Brig flood (Rotunno and Ferretti 2001). Expectedly, the sounding-derived temperature advection (Fig. 13b) shows there was warm air advection toward the mountains throughout the lowest 300 hPa of the troposphere, a common ingredient for heavy orographic precipitation (Lin et al. 2001). Figure 14 shows the NOWA-simulated accumulated precipitation on 21 October. Note that in this figure there was a precipitation maximum in excess of 90 mm located in the LMTA. Also note that the maximum that was located northwest of Corsica in the CTRL simulation (Fig. 9b) was not present in the NOWA precipitation field. This supports the arguments of Lin et al. (2005) and Reeves and Lin (2006), that lifting along the leading edge of the stable layer acted to trigger convection over the Ligurian Sea during IOP-8.

b. *Effects of differential advection*

Figure 15 shows backward trajectories of parcels ending at 1200 UTC 21 October at Milan both above the stable layer at 750 hPa (trajectory 1 in Fig. 15a) and below the stable layer at 950 hPa (trajectory 2 in Fig. 15a) for the CTRL simulation. Note that the parcel ending above the stable layer originated over the southern Mediterranean Sea while that ending below the inversion originated over the Italian peninsula. Notice that the lower parcel was apparently blocked by the northern Alps and deflected to the west. A comparison of soundings from these source regions (Fig. 15b) indicates that the thermodynamic profile over the Mediterranean Sea was both warmer and less stable than that over the Italian peninsula. The temperature advection at Milan at 1200 UTC 21 October (Fig. 15c) indicates that below about 900 hPa there was cold air advection, while above, there was warm air advection, consistent with the differential advection mechanism proposed by

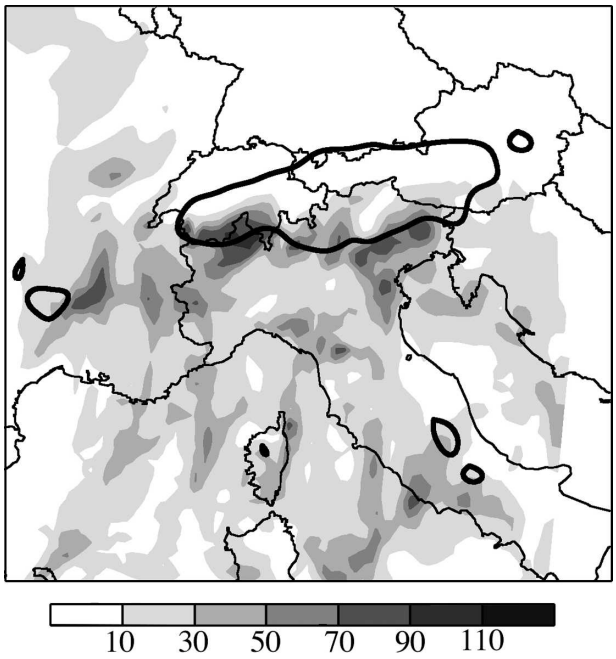

FIG. 14. NOWA-simulated 24-h accumulated precipitation (mm; shaded as in legend) on 21 Oct 1999.

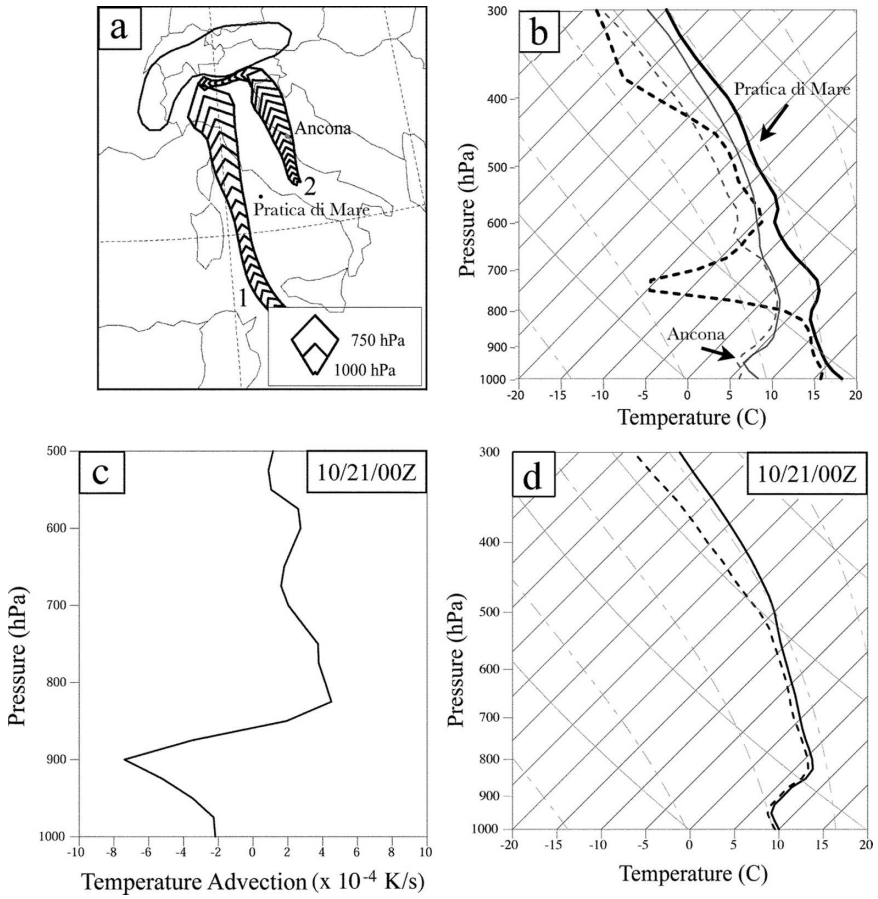

FIG. 15. CTRL output showing (a) backward trajectory analyses taken at 750 hPa (trajectory 1) and 950 hPa (trajectory 2) from Milan between 1200 UTC 21 Oct and 1200 UTC 21 Oct, (b) CTRL-simulated soundings taken from Pratica di Mare at 0600 UTC 21 Oct and Ancona [see (a) for locations] at 0000 UTC 21 Oct, (c) CTRL-simulated vertical profile of temperature advection ($\times 10^{-4}$ K s^{-1}) at Milan at 0000 UTC 21 Oct, and (d) CTRL-simulated Milan sounding at 1200 UTC 21 Oct.

Lin et al. (2005). Figure 15d shows the CTRL-simulated Milan sounding at 1200 UTC 21 October. There was still a strong inversion at this time located at about 800 hPa.

One might suppose that, if the Alps had not blocked the airstream approaching northern Italy from over the Adriatic Sea, then the longevity of the stable layer and the precipitation distribution would be quite different. This notion was tested in a simulation in which the northern Alps were removed (Fig. 16), while keeping everything else identical to the CTRL simulation. This simulation is referred to as the NONA simulation.

Figure 16 shows the NONA-simulated 925-hPa θ_e and wind fields. At 1200 UTC 18 October (Fig. 16a), the flow was easterly across northern Italy. Low-θ_e air was advected toward the western Alps and a low-θ_e pool of air was developing adjacent to the western Alps consistent with that in the CTRL simulation (Fig. 7b). Throughout 19 October (not shown), low-θ_e air continued to be advected toward the Po Valley, leading to further buildup of the cold dome along the western Alps. By 1200 UTC 20 October (Fig. 16b), the flow entering the Po Valley had shifted so that it was from the south. This higher-θ_e airstream advected the low-θ_e air out of the Po Valley. This is apparent through comparison of Figs. 16b and 7c. Notice that the θ_e values in the Po Valley for the CTRL simulation (Fig. 7c) were between 5 and 10 K cooler than those in the NONA simulation. By 0000 UTC 21 October (not shown), most of the low-θ_e air was advected out of Italy in the NONA simulation, with the exception of a small pocket of 300–305-K temperatures that still remained along the western Alps. During the next 12 h (Fig. 16c), this pocket of low-θ_e air was completely advected out of the region of interest. Because the cool, stable layer still formed over the Po Valley, it appears that the northern Alps

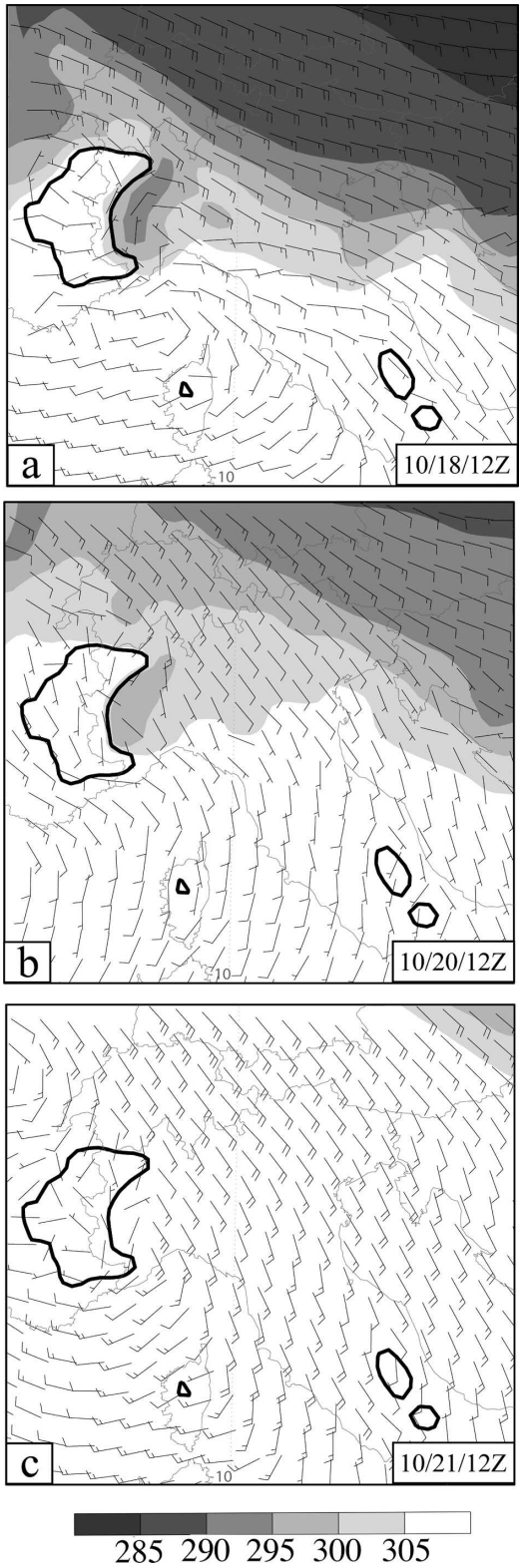

FIG. 16. NONA-simulated 925-hPa θ_e (K; shaded as in legend) and wind barbs (one-half barb is 5 m s^{-1}) at (a) 1200 UTC 18 Oct, (b) 1200 UTC 20 Oct, and (c) 1200 UTC 21 Oct. The 1-km terrain height is given by the thick contours.

were not responsible for stable-layer formation during IOP-8. However, as will be demonstrated below, blocking by the northern Alps did contribute to the maintenance of the stable layer.

The advection of the low-θ_e air out of the Po Valley, as noted in Fig. 16c, is also evident in the NONA-simulated Milan sounding at 1200 UTC 21 October (Fig. 17a) in which there is no inversion. This sounding is very similar to the 1200 UTC 21 October sounding from the NOWA simulation (Fig. 13a) in which the temperature profile was nearly moist neutral and the low-level flow was from the southeast. As a result, relatively warm air was advected into all layers above the Po Valley (Fig. 17b).

The 24-h accumulated precipitation for the NONA simulation on 21 October is shown in Fig. 18. The only heavy precipitation that occurred within the southern Alpine region during this period was along the southern slopes of the western Alps and Ligurian Apennines, where the incoming south-southeasterly flow approached the terrain at a nearly perpendicular angle and experienced vigorous vertical motion.

Comparing the results of the CTRL and NONA simulations, it appears that the northern Alps played a significant role in the stable-layer maintenance by acting to retain the low-θ_e air over northern Italy at earlier times and by blocking the relatively stable airstream impinging from over the Adriatic Sea at later times. As a result, the warm southerly flow approaching northwestern Italy from over the southern Mediterranean Sea was forced to ride up and over the cool pool of air, leading to the advection of warm, less stable air atop the cooler and more stable air mass in the Po Valley. This differential advection in the CTRL simulation appeared to help maintain the stable layer.

c. *Effects of latent cooling*

To test the effects of latent cooling on stable-layer formation and maintenance, a simulation was performed that was identical to the CTRL simulation except with the thermal effects of melting and evaporation suppressed. This simulation is referred to as the NOEM simulation. Without latent cooling, low-θ_e air was still advected across northern Italy from the east, blocked by the western Alps, and deflected toward the south between 1200 UTC 17 October and 0000 UTC 20 October. This is demonstrated in Fig. 19a, which shows the NOEM-simulated 925-hPa θ_e and wind fields. A comparison of this figure to Fig. 7 shows fair agreement in the θ_e values as well as the horizontal extent of the cold pool. At 1200 UTC 21 October (Fig. 19b), there was a pool of low-θ_e air positioned next to the

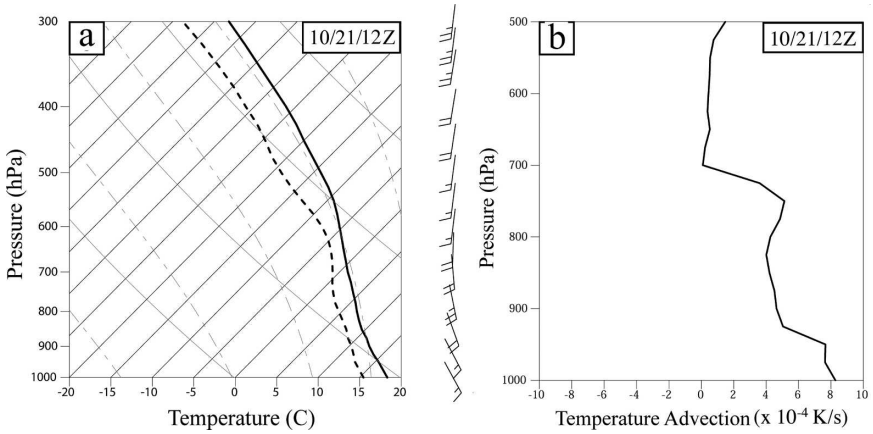

FIG. 17. NONA output showing (a) the Milan 0000 UTC 21 Oct sounding. Temperature is given by the solid lines and dewpoint temperature by the dashed lines. Wind speed and direction are denoted by the wind barbs to the right of each panel. One full barb is 10 m s^{-1}. (b) Vertical profile of temperature advection ($\times 10^{-4}$ K s^{-1}) at Milan at 0000 UTC 21 Oct.

western Alps, similar to that in the CTRL simulation (Fig. 7d).

The Milan sounding at 0000 UTC 21 October for the NOEM simulation is shown in Fig. 20a. As in the NOWA and NONA simulations, the Milan sounding was nearly moist neutral throughout the troposphere. Also note that the temperatures in the lowest 100 hPa of this sounding are about 5 K warmer than in the CTRL simulation (Fig. 15d). The temperature advection at Milan for the NOEM simulation is shown in Fig. 20b. Comparison of this profile to that for the CTRL simulation shows reasonable agreement, except that the cold air advection below 900 hPa was somewhat stronger in the CTRL simulation (Fig. 15c). The 24-h accumulated precipitation for the NOEM simulation is shown in Fig. 21. There was no maximum to the northwest of Corsica in this simulation, but there was a maximum of about 90 mm located in the LMTA.

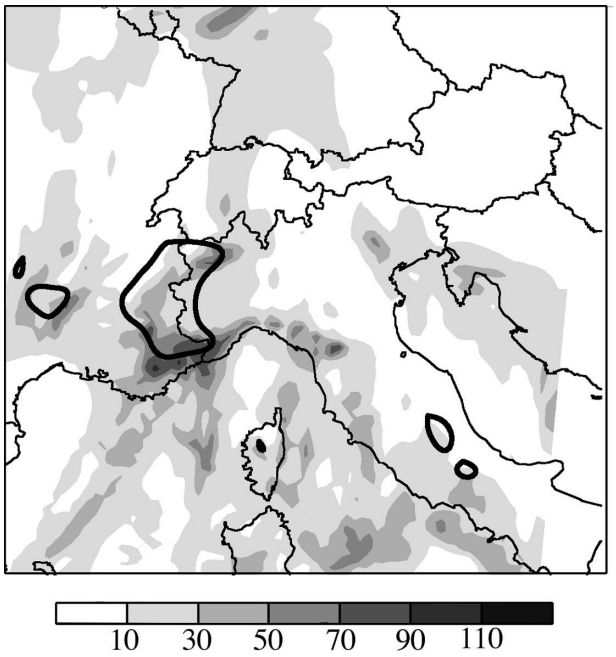

FIG. 18. NONA output showing the 24-h accumulated precipitation (mm; shaded as in legend) on 21 Oct 1999.

d. Effects of differential cloud cover

To test the effects of differential solar heating on the formation of the stable layer, another simulation was performed where the blocking of solar radiation by clouds was prohibited. Clouds were still allowed to form and precipitate in this simulation, which we will refer to as the NOCL simulation.

Figure 22 shows the NOCL-simulated 925-hPa θ_e and wind vectors. As in the CTRL simulation, there was easterly flow across the Po Valley at 1200 UTC 18 October (Fig. 22a) that advected low-θ_e air toward the western Alps. This tongue of low-θ_e air had temperatures that were between 2 and 5 K warmer than in the CTRL experiment (Fig. 7b). Wind vectors along the western Alps show that this low-θ_e air mass was deflected southward over the northern Ligurian Sea. Figure 22b shows that by 1200 UTC 21 October, the cold dome in the NOCL simulation had a similar horizontal extent as that in the CTRL simulation (Fig. 7d) but was, on average, 5 K warmer than that in the CTRL simulation.

The NOCL Milan sounding at 0000 UTC 21 October (Fig. 23a) shows that without cloud cover, the stable

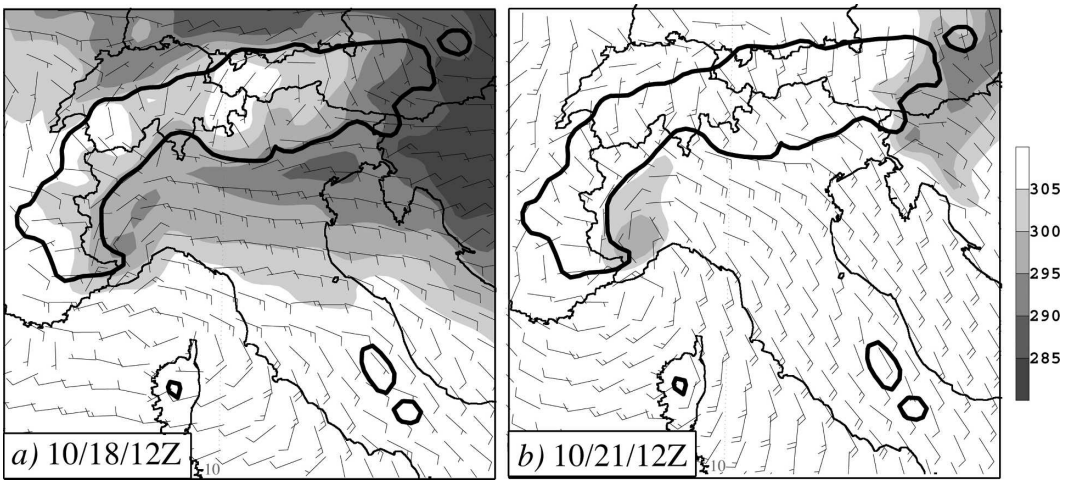

FIG. 19. NOEM-simulated 925-hPa θ_e (K; shaded as in legend) and wind barbs (one-half barb is 5 m s^{-1}) at (a) 1200 UTC 18 Oct and (b) 1200 UTC 21 Oct. The 1-km terrain height is given by the thick contours.

layer was about 2 K warmer at the surface than in the CTRL experiment (Fig. 8c) and only about 150 hPa deep, which is not as deep as that in the CTRL simulation. However, there is evidence of differential advection in the NOCL simulation as is demonstrated in Fig. 23b. This figure shows that there was cold air advection beneath the inversion (900 hPa) but that it was not as strong as in the CTRL simulation (Fig. 15c). Interestingly enough, the warm air advection above 900 hPa was not as strong as that in the CTRL simulation, either. The weaker warm air advection in the NOCL simulation can be understood through inspection of the NOCL 0000 UTC 21 October Milan sounding (Fig. 23a). The depth of the cold dome in the NOCL experiment was only about 100 hPa over the middle of the Po Valley, which is only about half the depth of the cold pool in the CTRL simulation. This was true throughout most of the Po Valley (not shown). Hence, incident airstreams to the cold dome in the NOCL simulation were not lifted as high as in the CTRL simulation. When we consider the Pratica di Mare, Italy, sounding shown in Fig. 15b, we can see that the level of free convection for this sounding was located at about 700 hPa. Hence, the lifting by the cold dome in the NOCL simulation appears to have been insufficient to bring parcels to their levels of free convection and incite convection. Ultimately, this led to less heating of the air parcels through condensation as they ascended over the cold dome.

The 24-h accumulated precipitation for the NOCL simulation is shown in Fig. 24. As in the CTRL simulation, there was a maximum to the northwest of Cor-

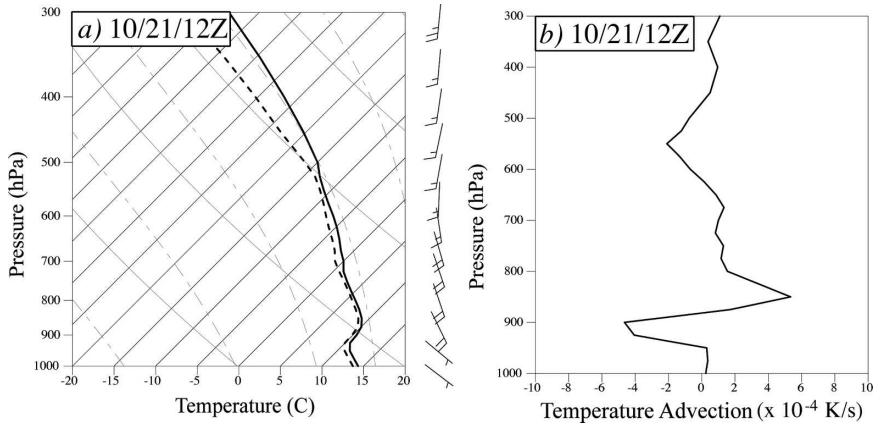

FIG. 20. NOEM output showing (a) the Milan 0000 UTC 21 Oct sounding. Temperature is given by the solid lines and dewpoint temperature by the dashed lines. Wind speed and direction are denoted by the wind barbs to the right of each panel. One full barb is 10 m s^{-1}. (b) Vertical profile of temperature advection ($\times 10^{-4}$ K s^{-1}) at Milan at 0000 UTC 21 Oct.

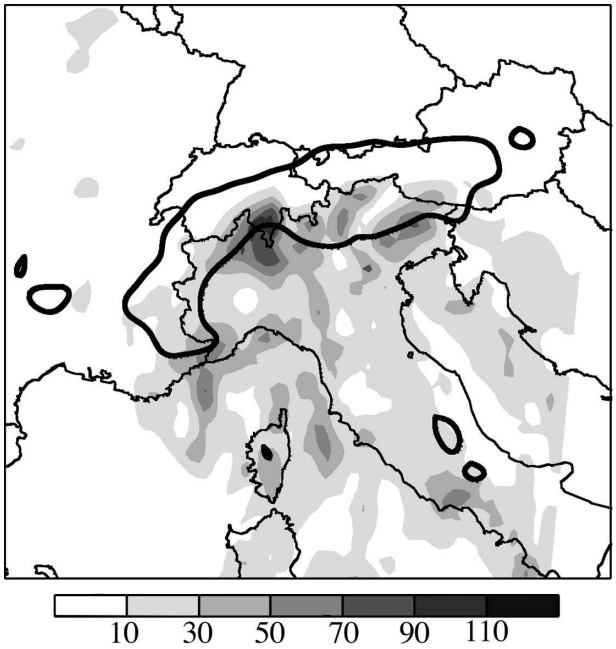

FIG. 21. NOEM output showing the 24-h accumulated precipitation (mm; shaded as in legend) on 21 Oct 1999.

sica; only in the NOCL simulation, this maximum was between 70 and 90 mm while in the CTRL simulation, it was in excess of 100 mm. The NOCL simulation also had a precipitation maximum greater than 90 mm in the LMTA area that did not exist in the CTRL simulation (Fig. 9b).

e. Effects of surface roughness

Xu (1990) noted in their idealized simulation of cold air damming that the longevity of stable layers increased as surface roughness was increased. To test the effects of surface roughness, an additional simulation was performed where the surface roughness over land was set to be equal to that over water (0.0001 m). We will refer to this simulation as the SMTH simulation.

Figure 25 shows the SMTH-simulated 925-hPa θ_e and winds. As in the CTRL simulation (Fig. 7), low-θ_e air was advected across the Po Valley toward the western Alps. As this air mass impinged on the western Alps, it was deflected southward (Fig. 25a). At 1200 UTC 18 October (Fig. 25b), the θ_e values within the cold pool were between 5 and 10 K cooler than in the CTRL simulation (Fig. 7b). This was because the smoother surface allowed for stronger low-level winds (note that in Fig. 25a the winds were between 5 and 10 m s^{-1} faster than in the CTRL simulation), thus building a more pronounced cold pool. By 1200 UTC 21 October (Fig. 25b), the low-θ_e air mass was mostly eroded in the SMTH simulation. At this time, temperatures in the western Po Valley were between 5 and 10 K *warmer* than in the CTRL simulation. Again, this appears to be related to the faster winds in the SMTH simulation compared with the CTRL simulation. Note also that in the LMTA, the flow does not appear to be blocked as in the CTRL simulation. Rather, it appears to be flowing up the mountain slope.

Figure 26a shows the SMTH-simulated Milan sounding at 0000 UTC 18 October. This sounding compares fairly well to that in the CTRL simulation (Fig. 8a) except that there was an inversion located just above 900 hPa in the SMTH simulation that was not present in the CTRL simulation this early. The SMTH-simulated Milan sounding at 0000 UTC 21 October (Fig. 26b) shows there was still an inversion in the SMTH simu-

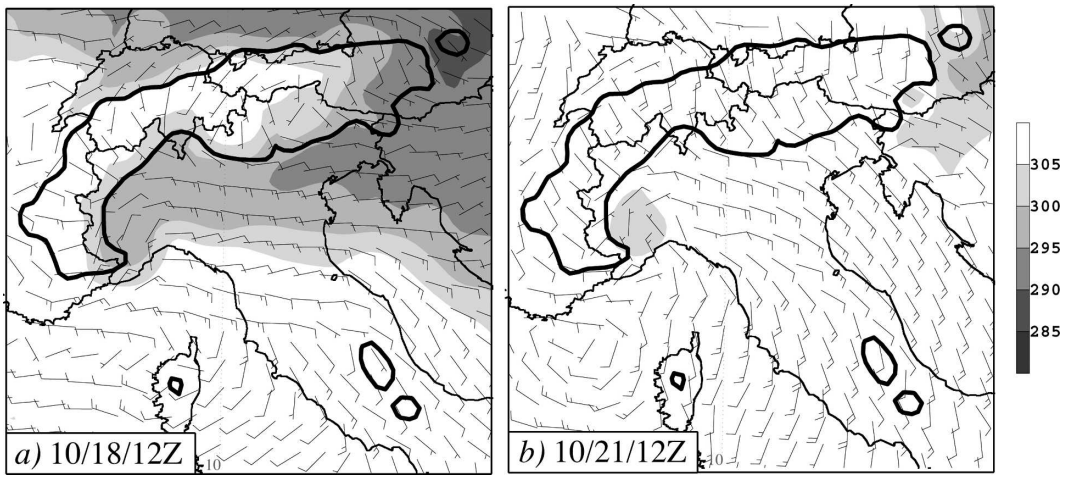

FIG. 22. NOCL-simulated 925-hPa θ_e (K; shaded as in legend) and winds (one-half barb is 5 m s^{-1}) at (a) 1200 UTC 18 Oct and (b) 1200 UTC 21 Oct.

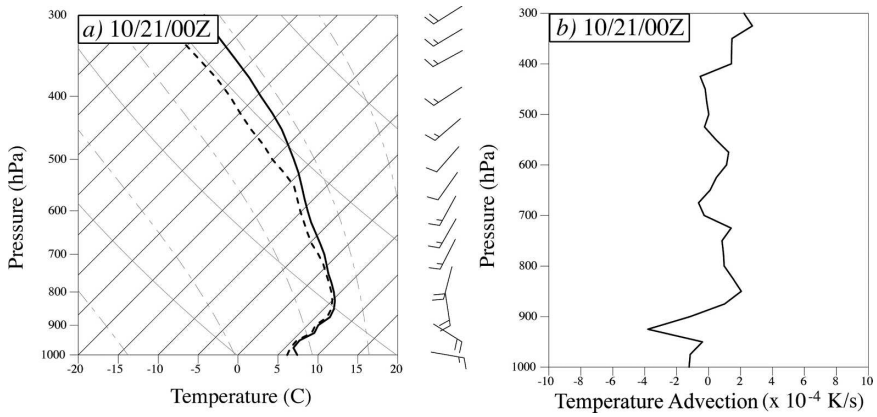

FIG. 23. NOCL-simulated (a) Milan sounding at 0000 UTC 21 Oct (one full barb is 10 m s^{-1}) and (b) vertical profile of temperature advection ($\times 10^{-4}$ K s^{-1}) at Milan at 0000 UTC 21 Oct.

lation, but that it was not as strong as that in the CTRL simulation (Fig. 8c). From the analyses presented in Figs. 25 and 26, we conclude that a reduced surface roughness acted to accelerate the formation of the stable layer at earlier times, ultimately leading to a stronger cold pool that, although it started to erode earlier, took marginally longer to erode.

The 24-h accumulated precipitation for the SMTH simulation is provided in Fig. 27. There was a precipitation maximum to the northwest of Corsica that was between 70 and 90 mm. More important though, is the large maximum in excess of 110 mm in the LMTA.

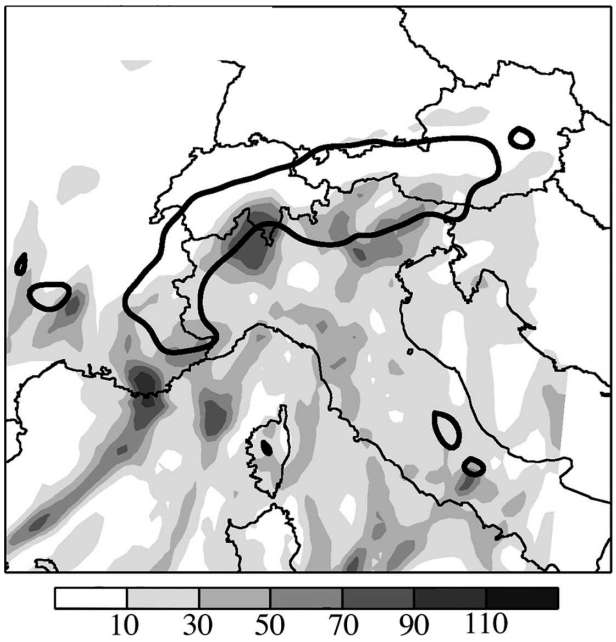

FIG. 24. NOCL-simulated 24-h accumulated precipitation (mm; shaded as in legend) on 21 Oct 1999.

This maximum is related to the upslope flow noted in Fig. 25b.

5. Discussions and conclusions

In this study, the mechanisms leading to the formation, maintenance, and erosion of the strong stable layer that developed over the Po Valley during IOP-8 of the MAP project were investigated. Previous research of IOP-8, as well as other cases of cold air damming suggest, there are a number of mechanisms that may have acted individually, or in concert, to form and maintain the stable layer. These mechanisms are orographic blocking, differential advection, latent cooling, differential cloud cover, and friction. The PSU–NCAR MM5 was used to simulate MAP IOP-8, and model sensitivity tests were performed to determine more precisely which mechanism(s) were dominant.

The control experiment with all the physical processes and complete topography reproduced the stable layer, flow patterns, and the precipitation distribution reasonably well. Trajectory analyses show the western Alps acted to block the impinging easterly flow and deflect it to the south. This blocking led to a significant buildup of low-θ_e air over the Po Valley up through 0000 UTC 20 October. Relatively warm, less stable airstreams approaching the Po Valley from the Mediterranean Sea were forced to ride up and over the cool layer. This produced differential advection of warmer and less stable air atop the cooler and more stable air in the Po Valley, which intensified the stable layer inversion and appeared to help maintain the stable layer.

The role of blocking by the western Alps was tested in a simulation where this portion of the terrain was removed. The results of this simulation indicate that the western Alps played a significant role in forming and

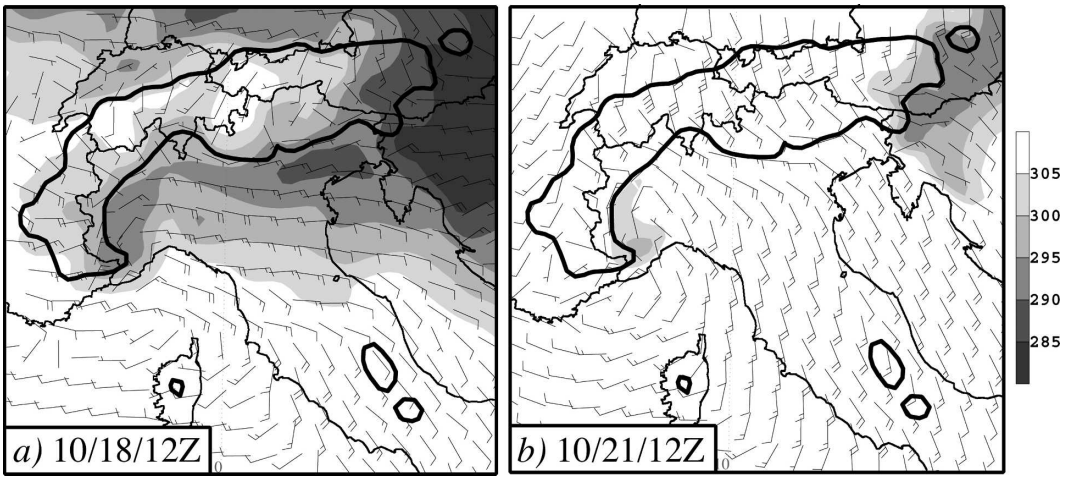

FIG. 25. SMTH-simulated 925-hPa θ_e (K; shaded as in legend) and winds (one-half barb is 5 m s^{-1}) at (a) 1200 UTC 18 Oct and (b) 1200 UTC 21 Oct.

maintaining the stable layer over the Po Valley. Without the western Alps present, low-θ_e air did not accumulate over the Po Valley. As a result, there was warm air advection in the Po Valley and significant precipitation accumulations occurred in the LMTA. The hypothesis that blocking by the western Alps and northern Alps acted to form and maintain the stable layer was tested through two sensitivity tests where the western Alps and the northern Alps were removed in turn. These sensitivity tests support the hypothesis

When latent cooling and the blocking of solar radiation by clouds were deactivated, the stable layer still formed in much the same manner as that in the CTRL simulation. However, the inversions in the Milan sounding for each of these tests were considerably weaker and stable-layer erosion occurred earlier than in the CTRL simulation. This led to smaller precipitation accumulations over the Ligurian Sea and greater precipitation accumulations over the LMTA. This connection between the stable-layer strength and the location of maximum convection and precipitation is consistent with the hypothesis of Smull et al. (2001) that the maximum precipitation and convection are shifted southward as the stable-layer strength is increased.

A final sensitivity experiment was performed where the surface roughness over land was set equal to that over water. In this simulation, the stable layer formed more quickly and was stronger than that in the CTRL simulation. The erosion process also appeared to start earlier in this simulation. However, because the stable layer was stronger, the erosion took longer in this simulation than it did in the CTRL simulation. We also noted that due to the decreased surface roughness, the low-level winds were stronger in the LMTA, and that at

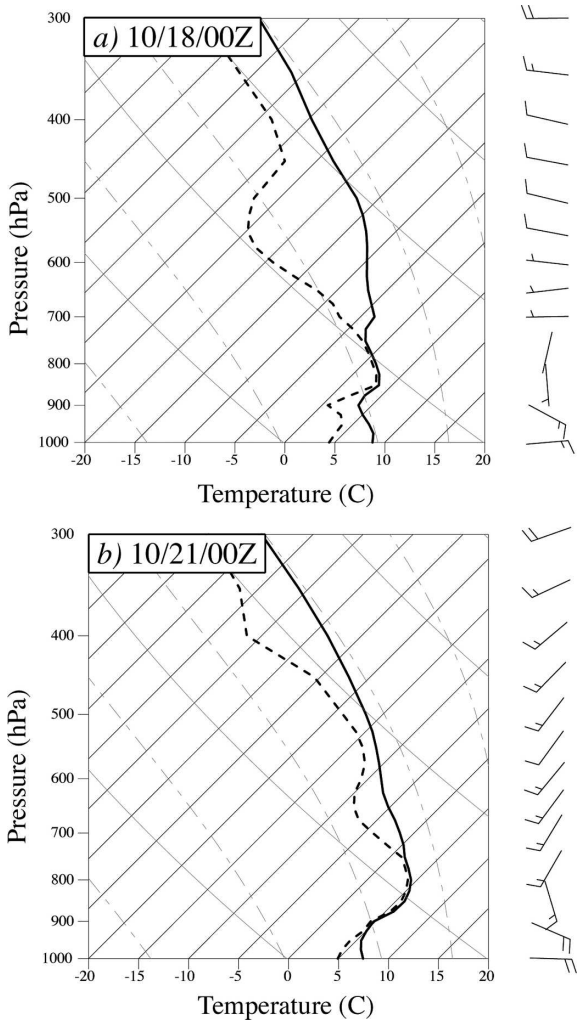

FIG. 26. SMTH-simulated Milan sounding at (a) 0000 UTC 18 Oct and (b) 0000 UTC 21 Oct (one full barb is 10 m s^{-1}).

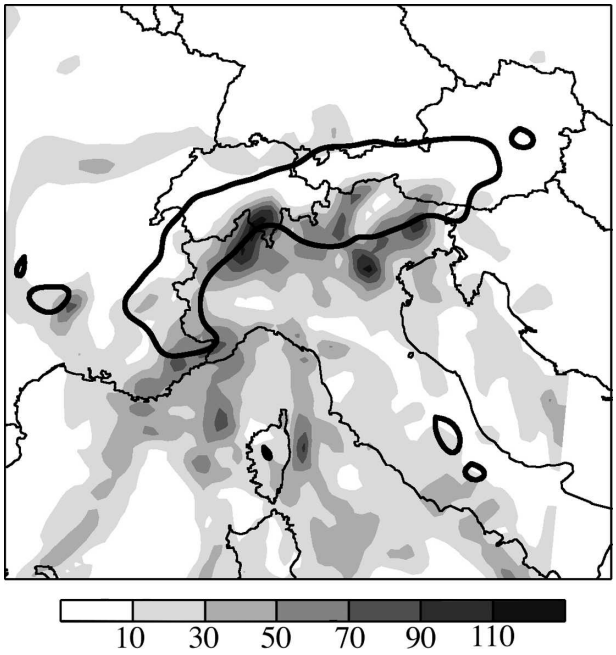

FIG. 27. SMTH-simulated 24-h accumulated precipitation (mm; shaded as in legend) on 21 Oct 1999.

later times in the simulation, flow in this area was not blocked by the orography, but flowed upslope instead. This resulted in a rather large precipitation maximum in excess of 110 mm in this location.

Overall, the stable-layer formation and maintenance appeared to develop in a series of steps. During the first stage, the easterly flow associated with the stationary high pressure center over northeastern Europe advected low-θ_e air across northern Italy and into the Po Valley. The western Alps blocked the low-θ_e air approaching from the east and deflected it toward the Ligurian Sea. This blocked flow led to a buildup of the low-θ_e air mass over the Po Valley. In the next stage, the western Alps and the northern Alps both acted to retain the low-θ_e air over the Po Valley. As a result, the warm southerly flow approaching northwestern Italy from over the southern Mediterranean Sea was forced to rise up and over the cool, stable layer leading to the differential advection of warmer and less stable air atop the cooler and more stable air in the Po Valley, which enhanced the inversion and helped to maintain the stable layer. One point of importance regarding the way in which this stable layer developed is that it did not follow the theoretical model of blocked-layer development in which the blocked layers form because the flow normal to the terrain has insufficient kinetic energy for it to ascend the orography (e.g., Xu 1990; Lin and Wang 1996). Rather, during IOP-8, the air that composed the blocked layer came from a different source region from the airstreams that were above the stable layer. Further research on stable layer development upstream of mountain ranges in other parts of the world where blocking is frequent is recommended to better understand this phenomena and its effects on the formation of convection.

The final note of significance regarding the findings of this research is that of the effects of the stable-layer strength on the precipitation distribution. In those simulations where the stable layer eroded earlier or was weaker than that in the CTRL simulation, the maximum northwest of Corsica was reduced and the maximum over the LMTA was increased. These findings are consistent with the idealized simulations of Reeves and Lin (2006) and, since the stable-layer strength was so strongly influenced by diabatic processes, these findings point to the importance of accurate representation of subgrid-scale processes in forecast models.

Acknowledgments. The authors thank Ólafur Rögnvaldsson, Gary Lackmann, and two anonymous reviewers. This work is supported by NSF Grant ATM-0344237. Computing was performed on the NCSU PAMS Linux cluster.

REFERENCES

Bell, G. D., and L. F. Bosart, 1988: Appalachian cold-air damming. *Mon. Wea. Rev.,* **116,** 137–161.

Betts, A. K., and M. J. Miller, 1993: The Betts–Miller scheme. *The Representation of Cumulus Convection in Numerical Models, Meteor. Monogr.,* No. 46, Amer. Meteor. Soc., 107–121.

Blackadar, A. K., 1979: High resolution models of the planetary boundary layer. *Advances in Environmental Science and Engineering,* J. R. Pfafflin and E. N. Ziegler, Eds., Vol. 1, Gordon and Breach, 50–85.

Bousquet, O., and B. F. Smull, 2003: Observations and impacts of upstream blocking during a widespread orographic precipitation event. *Quart. J. Roy. Meteor. Soc.,* **129,** 391–409.

Dudhia, J., 1993: A nonhydrostatic version of the Penn State–NCAR mesoscale model: Validation tests and simulation of an Atlantic cyclone and cold front. *Mon. Wea. Rev.,* **121,** 1493–1513.

Fritsch, J. M., J. Kapolka, and P. A. Hirschberg, 1992: The effects of subcloud-layer diabatic processes on cold air damming. *J. Atmos. Sci.,* **49,** 49–70.

Grell, G. A., 1993: Prognostic evaluation of assumptions used by cumulus parameterizations. *Mon. Wea. Rev.,* **121,** 764–787.

——, J. Dudhia, and D. R. Stauffer, 1994: A description of the fifth-generation Penn State/NCAR mesoscale model (MM5). NCAR Tech. Note NCAR/TN-398+STR, 138 pp.

Grossman, R. L., and D. R. Durran, 1984: Interaction of low-level flow with the Western Ghat mountains and offshore convection in the summer monsoon. *Mon. Wea. Rev.,* **112,** 652–672.

Houze, R. A., Jr., and S. Medina, 2005: Turbulence as a mechanism for orographic precipitation enhancement. *J. Atmos. Sci.,* **62,** 3599–3623.

Koch, S., M. desJardins, and P. J. Kocin, 1983: An interactive

Barnes objective map analysis scheme for use with satellite and convectional data. *J. Climate Appl. Meteor.,* **22,** 1487–1503.

Kusunoki, K., M. Mirakami, M. Hoshimoto, N. Orikasa, Y. Yamada, H. Mizuno, K. Hamazu, and H. Watanabe, 2004: The characteristics and evolution of orographic snow clouds under weak cold advection. *Mon. Wea. Rev.,* **132,** 174–191.

Lin, Y.-L., and T.-A. Wang, 1996: Flow regimes and transient dynamics of two-dimensional stratified flow over an isolated mountain ridge. *J. Atmos. Sci.,* **53,** 139–158.

——, R. D. Farley, and H. D. Orville, 1983: Bulk parameterization of the snow field in a cloud model. *J. Climate Appl. Meteor.,* **22,** 1065–1092.

——, S. Chiao, T.-A. Wang, M. L. Kaplan, and R. P. Weglarz, 2001: Some common ingredients for heavy orographic rainfall. *Wea. Forecasting,* **16,** 633–660.

——, H. D. Reeves, S.-Y. Chen, and S. Chiao, 2005: Formation mechanisms for convection over the Ligurian Sea during MAP IOP-8. *Mon. Wea. Rev.,* **133,** 2227–2245.

Medina, S., and R. A. Houze Jr., 2003: Air motions and precipitation growth in Alpine storms. *Quart. J. Roy. Meteor. Soc.,* **129,** 345–372.

——, B. F. Smull, R. A. Houze, and M. Steiner, 2005: Cross-barrier flow during orographic precipitation events: Results from MAP and IMPROVE. *J. Atmos. Sci.,* **62,** 3580–3598.

Neiman, P. J., F. M. Ralph, A. B. White, D. E. Kingsmill, and P. O. G. Persson, 2002: The statistical relationship between upslope flow and rainfall in California's coastal mountains: Observations during CALJET. *Mon. Wea. Rev.,* **130,** 1468–1492.

Reeves, H. D., and Y.-L. Lin, 2006: Effect of stable layer formation over the Po Valley on the development of convection during MA *J. Atmos. Sci.,* **63,** 2567–2584.

Rotunno, R., and R. Ferretti, 2001: Mechanisms of intense Alpine rainfall. *J. Atmos. Sci.,* **58,** 1732–1749.

——, and ——, 2003: Orographic effects on rainfall in MAP cases IOP2B and IOP8. *Quart. J. Roy. Meteor. Soc.,* **129,** 373–390.

Smull, B. F., O. Bousquet, and D. Löthi, 2001: Evaluation of real-time MC2 simulation results for a case of significant upstream blocking during MAP. *MAP Newsletter,* Vol. 15, Meteo-Swiss, Zurich, Switzerland, 84–87.

Steiner, M., O. Bousquet, R. A. Houze Jr., B. F. Smull, and M. Mancini, 2003: Airflow within major Alpine river valleys under heavy rainfall. *Quart. J. Roy. Meteor. Soc.,* **129,** 411–431.

Tao, W.-K., and J. Simpson, 1993: Goddard cumulus ensemble model. Part I: Model description. *Terr. Atmos. Oceanic Sci.,* **4,** 35–72.

Wolyn, P. G., and T. B. McKee, 1989: Deep stable layers in the intermountain western United States. *Mon. Wea. Rev.,* **117,** 461–472.

Xu, Q., 1990: A theoretical study of cold air damming. *J. Atmos. Sci.,* **47,** 2969–2985.